3D printed microneedles for insulin skin delivery

Cristiane Patricia Pissinato Pere[1], Sophia N. Economidou[1], Gurprit Lall[1], Clémentine Ziraud[3], Joshua S. Boateng[2], Bruce D. Alexander[2], Dimitrios Lamprou[1], Dennis Douroumis[2*]

[1] School of Pharmacy, University of Kent, Chatham Maritime, Chatham, Kent, ME4 4TB, UK

[2] Faculty of Engineering and Science, School of Science, University of Greenwich, Chatham Maritime, Chatham, Kent ME4 4TB, UK

[3] Polytech Marseille Filière Matériaux : Luminy case 925 - 13288 Marseille Cedex 09, France

---

[*] Correspondence: Faculty of Engineering and Science, University of Greenwich, Medway Campus, Chatham Maritime, Kent ME4 4TB, UK. Tel.: +44 (0) 208 331 8440; Fax: +44 (0) 208 331 9805.
E-mail address: D.Douroumis@gre.ac.uk

ABSTRACT

In this study, polymeric microneedle patches were fabricated by stereolithography, a 3D printing technique, for the transdermal delivery of insulin. A biocompatible resin was photopolymerized to build pyramid and cone microneedle designs followed by inkjet print coating of insulin formulations. Mannitol, trehalose and xylitol were used as drug carriers with the aim to preserve insulin integrity and stability but also facilitate rapid release rates. Circular dicroism and Raman analysis demonstrated that all carriers maintained the native form of insulin with xylitol presenting the best performance. Franz cell release studies were used for in vitro determination of insulin release rates in porcine skin. Insulin was released rapidly within 20 min irrespectively of the microneedle design. 3D printing was proved an effective technology for the fabrication of biocompatible and scalable microneedle patches.

1. Introduction

Over the last 20 years transdermal microneedles (MNs) have paved the way for the delivery of various active substances across the skin, (Alkilani et al., 2015; Sanjay et al., 2017). These miniature devices are used for the administration of active drug substances, vaccines, including genetic material such as RNA and DNA (Chen et al., 2016). MNs can pierce skin in a painless way and, through the penetration of the stratum corneum, they unload the drug substance into the dermis. The minimally invasive administration of MNs has shown to improve systemic drug adsorption and thus bioavailability (Wermeling et al., 2008). Ideally, they provide improved patient compliance as they do not stimulate nerves associated with pain and can be self-administrated (Kaushik et al., 2001). MNs are classified into four categories including solid, coated, hollow, hydrogel - forming and dissolvable microneedles and are usually made of metal, polyscharides or polymeric materials (Ita, 2015).

Recent advances in skin delivery mediated by MNs involve the development of polyvinylpyrrolidone (PVP) and trehalose dissolvable MNs for the encapsulation of peptides. The MNs achieved rapid systemic delivery by dissolving in the interstitial fluid of the skin and retained the antimicrobial activity of the peptide (Dillon et al., 2017). In another study, MNs made by chitosan and beta-sodium glycerophosphate showed efficient delivery of levonorgestrel in vivo without causing any skin irritation. The pharmacokinetic profile of the drug presented similarities with the respective one of oral suspension, demonstrating that drug-loaded dissolving MN systems are an appealing alternative to traditional levonorgestrel administration routes (Yao et al., 2017). In another study, MNs were coated with 60 μg of a plasmid DNA cocktail encoding the Leishmania infantum nucleosomal histones H2A, H2B, H3 and H4 and their immunization capacity was compared against subcutanenous or intradermal injection of the plasmid. The results demonstrated that MNs improved immunogenicity, but higher plasmid doses might be required for better Leishmania control (Moreno et al., 2017).

Significant efforts have been placed in the skin delivery of insulin analogs by using MNs in order to address the accuracy of the injections, decrease leakage of insulin to the skin surface, and reduce pain caused by repeated injections (Guo and Wang, 2017; Narayan, 2014). In a recent study, MNs for insulin delivery, composed of modified alginate and hyaluronate, were fabricated by micromoulding (Yu et al., 2017). The optimized MNs showed good mechanical strength and good piercing capacity while insulin bioactivity was not affected. In vivo studies demonstrated a sustained hypoglycemic effect with high relative pharmacologic availability and relative bioavailability, compared to subcutaneous injections. Clinical studies in diabetic Sprague – Dawley rats demonstrated effective hypoglycemic control when insulin was released from calcium sulfate and gelatine biodegradable composite microneedle patches, showing that insulin is a suitable candidate for MN-mediated transdermal delivery (Yu et al., 2017).

However, there are several pitfalls in MN skin delivery related to the manufacturing process and materials used for the development of MN patches. Micromoulding is the most common approach used for the fabrication of dissolving and gel forming MNs and involves a sequence of time-consuming and difficult to scale-up steps. On the other hand, coating technologies do not always result in uniform, accurate and reproducible active coated layers and fail to avoid drug deposition on the MNs substrate. There are also serious concerns regarding the biocompatibility, skin irritation and even sterilization issues (McCrudden et al., 2015) of the materials (e.g. silicon, polymers) used for MNs fabrication as most of them are suitable for oral use but not approved for skin delivery. The limited loading of active substances in most of these MN technologies is another shortcoming for efficient transdermal delivery. More explicitly, coating techniques limit the drug amount that can be loaded in the system to 1 mg maximum (Kim et al., 2012) while larger amounts (up to 33 mg) have been successfully delivered by dissolving MN (McCrudden et al., 2014).

3D printing or additive manufacturing is a family of technologies that employ a virtual Computer Aided Design (CAD) model to create a physical object through the consecutive creation of layers. It was launched in 1980s (Kodama, 1981; Hull, 1984) and it has revolutionized the field of pharmaceutical, biomedical and material sciences due to the capabilities for rapid and cost-effective prototyping of complex structures (Pedde et al., 2017).3D printing endows the prototyping and fabrication process with versatility; objects are manufactured in a one-step fashion with high degrees of complexity and reproducibility. .

Among the various technologies that comprise 3D printing, photopolymerisation-based techniques enable the fabrication of structures through the consecutive layer-wise polymerization of UV-sensitive polymers, through a curing process named photopolymerization. Stereolithography (SLA), Digital Light Processing (DLP) and Two-Photon-Polymerization (2PP) are among these technologies (Economidou et al., 2018). In the field of TDD, Gittard et al. employed a photopolymerisation-based printer (DLP) to fabricate MNs of various geometries for wound healing applications followed by pulse laser deposition of silver and zinc oxide thin films (Gittard et al., 2011). Similarly, Lu et al. incorporated Dacarbazine (1-2%) a skin anticancer drug into poly(propylene fumarate)/drug blends followed by photopolymerization through a micro-stereolithographic (DLP) apparatus thatbuilt the MN arrays (Lu et al., 2015).

In this study, we employed SLA to fabricate MN arrays of different designs followed by inkjet printing of insulin – polyscharide films. 3D printed patches, featuring MN with cone and pyramid geometries, were made using a Class 1 biocompatible resin with excellent mechanical strength and piercing capacity. Mannitol, trehalose and xylitol, were used as insulin carriers at different wt/wt ratios in order to preserve insulin activity prior the application of uniform and accurate "active" coating on the MN surface.

2.   Materials and Methods

Insulin solution from bovine pancreas (10 mg mL^{-1}) and trehalose dihydrate were purchased from Sigma-Aldrich (Gillingham, UK), while Xylisorb® 90 (Xylitol) and Pearlitol® (mannitol) were kindly donated by Roquette Freres (France). The printing polymer

was the biocompatible Class I resin, Dental SG, procured by Formlabs. All solvents were of analytical grades.

2.1 3D printing of microneedles

Two different MN designs, pyramid and cone, were developed using appropriate engineering software (SolidWorks by Dassault Systems), featuring square and circular cross-sections, respectively. The length of all MNs was 1 mm while the dimensions of the base cross-sections were 1x1 mm for the pyramid and ø 1 mm for the cone. The MNs were built as attached to a solid 15x15x1 mm substrate, forming patches of 48 MNs each. The arrays were fabricated using a Form 2 stereolithography (SLA) printer by Formlabs, with high resolution capabilities (25 and 140 microns for z and x axes, respectively). To obtain higher mechanical properties, the MN arrays, after being washed in isopropyl alcohol to remove excess resin, were cured under ultraviolet radiation for 60 minutes at 40ºC (MeccatroniCore BB Cure Dental station).

2.2 Inkjet printing of insulin formulations microneedles

The insulin solutions were printed onto each MN surface in the form of fine droplets using an inkjet printer (NanoPlotter II, Gesim, Germany) through a piezo-driven dispenser (PicPip 300). All MN arrays were positioned at 45º relative to the dispenser and for each coating cycle, 10 dots of 2 droplets of a coating formulation were dispensed longitudinally to the axis of each MN. The process was repeated for 92 jetting cycles resulting in 10 UI (350 µg) of insulin/array. Solvent (de-ionised water) was evaporated to produce uniform and reproducible solid thin films on the MNs after 24 hr of incubation at room temperature. For the purposes of the study three coating formulations were used, consisting of insulin:xylitol (5:1 wt/wt), insulin: mannitol (5:1 wt/wt) and insulin:trehalose (5:1 wt/wt) as 2% solid content.

2.3 Scanning electron microscopy

The coated MN arrays were mounted onto aluminium stubs using a double-sided carbon adhesive tape (Agar scientific, UK). Each coated cross-MN array was examined by SEM (Hitachi SU 8030, Japan) using a low accelerating voltage (1.0kV). A low accelerating voltage was used to avoid electrical charges on the cross-MNs. The images of coated cross-MNs were captured digitally from a fixed working distance (11.6 mm) using different magnifications (30, 80, 110 or 120 x).

2.4 Circular Dicroism (CD) analysis

The formulations were diluted to 1.0 mg mL-1 in deionized water and the spectra were recorded at 20ºC between 190 and 260 nm by circular dichroism (Chirascan, Applied Photophysics, UK) using a 0.1 mm polarization certified quartz cell (Hellma). Spectra were recorded using a step size of 1 nm, a bandwidth of 1 nm and an acquisition time of 1 second. Four scans were recorded for each sample and averaged and a corresponding spectrum of water was subtracted from each spectrum. For estimation of the secondary structural composition of insulin, the CD spectra were evaluated using CDSSTR method (Sreerama and Woody, 2000).

2.5 Raman analysis

The films of the formulations and their respective components were analysed using Raman microscopy (Jobin Yvon LabRam I) with a laser of 532 nm wavelength coupled with an optical microscope to a 50x objective.

2.6 Penetration of MN in porcine skin

The necessary force required to pierce the skin has been found to be straightforwardly affected by the geometry of the MNs (Davis et al., 2004). In this study, to determine the effect of needle shape on the force required for skin penetration, piercing tests using porcine skin were conducted. In order to have a frame of reference with respective literature, metallic MN arrays were tested as well, the fabrication and physical characteristics of which, are described elsewhere (Ross et al., 2015). A texture analyser was employed, and the MN array was mounted on the moving probe using double-sided adhesive tape. Prior to testing, the porcine skin samples were placed in waxed petri dishes. Continuous force and displacement measurements were recorded to identify the point of needle insertion. The speed of the moving probe was 0.01mm/s.

2.7 *In vitro* release of insulin coated MNs

Release studies of insulin were undertaken in abdominal porcine skin using Franz diffusion cells (PermeGear, Inc., PA, USA). Full thickness abdominal porcine skin was collected from a local slaughterhouse (Forge Farm Ltd, Kent, UK). The abdominal hair was shaved using a razor blade. Collected skin was stored at 4ºC until it was used. A total diffusion area of 1.1 cm^2 was used to assess insulin release into abdominal porcine skin. Skin (750 µm thick) was cut for permeability studies of insulin using a dermatome instrument (Padgett dermatome or blade, USA). Skin samples were then placed in phosphate buffered saline (PBS) (pH 7.4) for 1 hr before *in vitro* studies. The MN arrays were inserted into abdominal porcine skin (900 µm) for 30 s using manual finger pressure. A skin pierced cross-MN array was mounted onto the donor compartment of a Franz diffusion cell. The temperature of the Franz cells was maintained at 37ºC using an automated water bath (Thermo Fisher Scientific, Newington, USA) whilst the skin temperature was maintained at 32ºC using a digital thermometer (Fisher Scientific, UK). Sample fractions (6-6.5 ml/hr) were collected using an auto-sampler (FC 204 fraction collector, Gilson, USA) attached to the Franz diffusion cells. Statistical analysis for the drug release was performed by using a Mann−Whitney nonparametric test and t test analysis for the in vivo studies (InStat, GraphPad Software Inc., San Diego, CA, USA), where samples are considered to be statistically significant at $p < 0.05$.

2.9 Skin preparation for in-vitro MN testing

The fatty tissue below the abdominal area of porcine skin was removed with scalpel and then pinned onto polystyrene block and wiped with 70 % ethanol. The skin was then cut at 1mm by applying the dermatome at an angle of ±45° (Padgett dermatome, Integra LifeTMSciences Corporation USA). The thickness of skin was measured by using a calliper and the tissue disks

of the required dimensions were cut for the Franz diffusion cells using a scalper. The skin tissue (0.9–1.1 mm thick) was placed onto filter paper soaked in a small amount of saline phosphate buffer pH 7.4 for 2 h.

2.10 HPLC analysis

The amount of insulin collected from the receptor fluid was determined by HPLC (Agilent Technologies, 1200 series, Cheshire, UK) equipped with a Phenomenex Jupiter 5u c18 300 Å, LC Column (250×4.60 mm, particle size 5 μm, Macclesfield, UK). The mobile phase consisted of water with 0.1 % TFA and acetonitrile with 0.1%TFA (66:34v/v), with a 1 mL min^{-1} flow rate. The column was equilibrated at 35°C, the injection volume was 20 μL and the eluent was analysed with a UV detector at 214 nm. The results were integrated using Chemstation® software.

3. Results and discussion

MN arrays with cone- and pyramid-shaped needles were successfully printed using an additive manufacturing technique known as stereolithography. The SLA processes a Class I biocompatible resin to build up structures in a layer – by – layer manner from computer aided design (CAD) models. Dental SG resin is one of the few commercially available, biocompatible, FDA certified polymers that are compatible with stereolithography printers and the only Class I compatible with the Form2 system. After printing, the MN arrays were cured using a light source – UV laser to harden the plastic MN patches through a photopolymerization process resulting in improved mechanical properties. As shown in Fig. 1 SLA produced two different designs of pyramid (6x8) and cone–shaped (6x8) MN patches with 1000μm height, 1000μm width and 1.85mm interspacing distance (measured from tip-to-tip). In Fig. 1c,d the build layers of both MN designs appear highly consistent and reproducible. The high resolution of the printer permitted the reproducible fabrication of arrays in excellent detail, leading to the formation of sharp needle tips that favour the skin insertion. The low cost of the printing material and the fast production speed renders SLA an attractive process for MN fabrication. Quantitively, the currently available commercial SLA apparatuses have a limited print volume which for Form 2 is $145 \times 145 \times 175$ mm. This print volume allows the manufacturing of up to 49 MN arrays according to the dimensions and methodology described in approximately two hours. Upscaling of the process at a manufacturing scale depends on the introduction of printers with larger print volumes. However, considering the low cost of these printers and the small fabrication time, parallel printings in multiple printers can generate a great number of arrays fast and accurately.
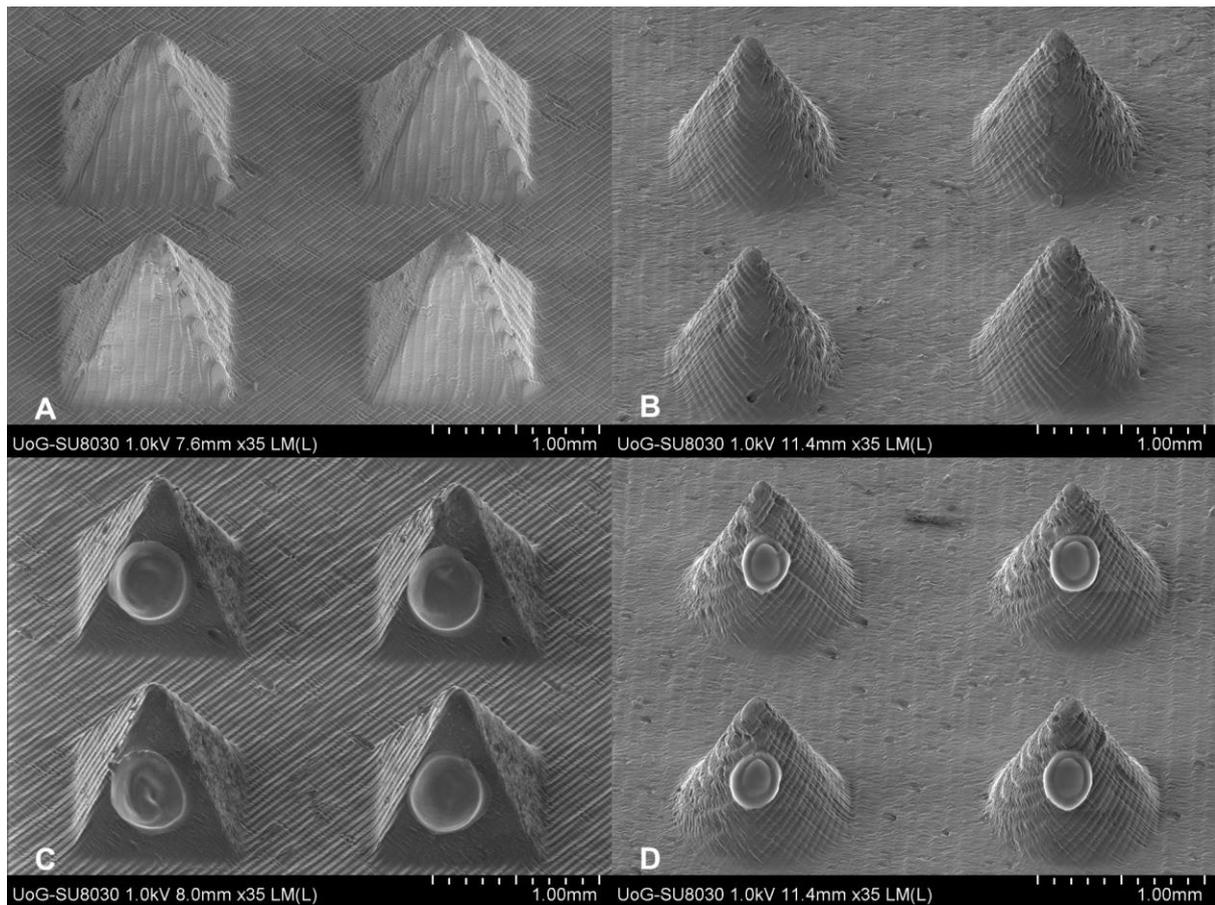
Fig. 1 SEM images of 3D printed microneedle designs of a) plain pyramid, b) plain cone, c) insulin coated pyramid and c) insulin coated cone.

Inkjet printing was then employed to apply coatings of insulin and sugar alcohol solutions through a piezoelectric dispenser. This 2D printing approach has been previously used for coating of metal MNs(Ross et al., 2015; Uddin et al., 2015) where by optimizing the applied voltage (mV) and the pulse duration (ms) droplets of 300 pL volume with consistent particle size of $100 - 110$ μm as observed by the printer's stroboscope, were produced. The dispenser's tip (50μm) was kept close to the microneedle surface to avoid losses of the coating material. Fig. 2 shows the morphologically excellent coatings on the MN surface without the presence of any satellite droplets on the substrate. In addition, the inkjet printing led to the formation of uniform layers with high precision and reproducibility without the creation of bulky coatings observed in conventional techniques such as dip coating.

Regarding the stability and storage requirements of the coated MN arrays, to the authors' knowledge insulin is not thermostable and so insulin coated microneedles should follow the same insulin manufacturers' requirements for storage at 2° to 8°C. The medium and long-term stability of insulin as coating formulation for microneedles needs to be explored more thoroughly, even though the used sugars are commonly employed as stabilizing agents and cryoprotectants for proteins and biological products.

Fig. 2: Inkjet coating process of 3D printed microneedles.

The coating formulations consisted of insulin solutions of two alcohol sugars (xylitol, mannitol) and disaccharide (trehalose) specifically selected as drug carries. The selection of those excipients was twofold, firstly because they favour and enhance insulin stability in solid state and secondly because we anticipated a rapid coating dissolution immediately after the MN piercing (Yong et al., 2009; Kim et al., 2009; Schiffter et al., 2010).

Circular Dichroism

Circular dichroism (CD) is a well-known spectroscopic technique used to study the secondary structure of proteins and polypeptides in solution. In order to investigate the effect of different sugars on the structure of insulin, CD experiment was carried out. The secondary structure of insulin in all samples was also estimated by the CDSSTR method (Sreerama and Woody, 2000) and it is quantitatively summarized in Table 1.

In Fig. 3 all far-UV CD spectra of insulin and insulin-sugar formulations showed two negative minima around 210 and 225 nm commonly associated with predominant features of α-helices structure which is in close agreement with the spectra already reported in the literature (Ettinger and Timasheff, 1971; Sarmento et al., 2007; Yong et al., 2009; Andrade et al., 2015). Also, the secondary structure of pure insulin in solution estimated by CDSSTR method, agree well with that obtained by others (Melberg and Johnson 1990; Yong et al. 2009). The spectra of insulin-mannitol and insulin-trehalose show a slightly decrease in the absolute intensities at 210 and 225 nm which can indicate changes in the ratio of α-helix and β-sheet content. According to the secondary structure estimation these changes do indicate a decrease in α-helix content of 4 and 5% for mannitol and trehalose formulations respectively, with a simultaneously increase of 4% in the β-sheet. Although, similar effect of trehalose on α-helix content was reported by Yong et al. (Yong et al., 2009), the reason for this is still unclear and further research is needed.

Among the tested sugars, xylitol presented the best capability to maintain insulin in its native form with almost the same amount of α-helix content.
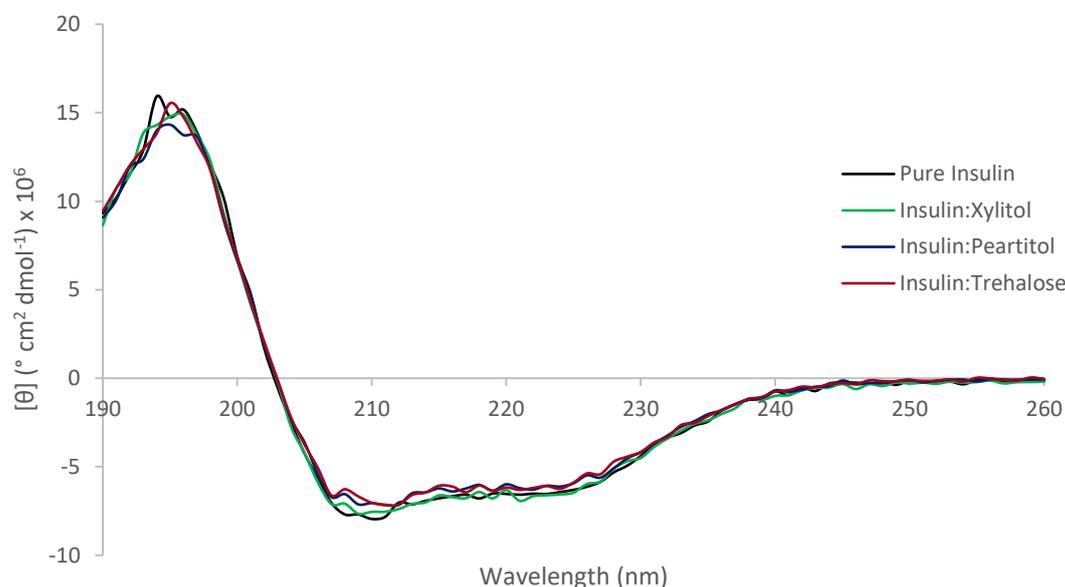

Fig. 3: CD of insulin and insulin formulations

Table 1: Secondary structure prediction by CDSSTR using far-ultraviolet CD spectra.

	Insulin	Insulin:Xylitol 5:1	Insulin:Mannitol 5:1	Insulin:Trehalose 5:1
Alpha Helix	58%	57%	54%	53%
β-Sheet	7%	7%	10%	10%
Turn	10%	11%	11%	11%
Random coil	26%	26%	26%	26%

Raman spectroscopy

Raman spectroscopy has been widely used to study possible changes in chemical composition as well to study important information about protein conformation.

In this study, the spectrum of native insulin, Fig. 4, shows a strong amide I band at 1661 cm^{-1} and a shoulder near 1682 cm^{-1} (CO stretching with some contribution from the stretching of CN groups and CCN deformations) which are indicative of α-helix structure and random coil form, respectively, being in accordance with Yu et al. (Yu et al., 1972).

All insulin formulations spectra display a similar band shape to the native insulin, assigning the α-helix structure. However, insulin-xylitol and insulin-mannitol formulation display a shift toward greater frequency, 1663 cm^{-1} and 1662 cm^{-1}, respectively, and insulin-trehalose was shifted to lower frequency at 1658 cm^{-1}. Furthermore, for mannitol formulation, an increase the amide I peak absorbance was seen while a pronounced decrease was noted for trehalose one. Those changes might be due the different effect of each sugar on the vibrational spectra of insulin as well on the intra- and inter-chain couplings between the adjacent peptide

units as stated by Carpenter and Crowe (Carpenter and Crowe, 1989) and Souillac et al. (Souillac et al., 2002).

Characteristic peaks of sugars were not found in Raman spectra due to the fact that insulin is more concentrated in the formulations films compared to the carbohydrate films and XRD analysis (data not shown) suggested that the sugar were amorphous and therefore is likely to afford a weak Raman spectrum. It has also been suggested that there is also hydrogen bond between the sugar and the dried protein as reported by Carpenter and Crowe (Carpenter and Crowe, 1989). This interaction is known as water-replacement mechanism and it is responsible for preventing protein denaturation by replacing water molecules with other hydrogen bond reducing then the probability of protein aggregation during the drying process.(Souillac et al., 2002)Therefore, our results show the developed formulations have good capability to maintain insulin molecule in its native form with high amounts of α-helix content which is essential for its biological activity.
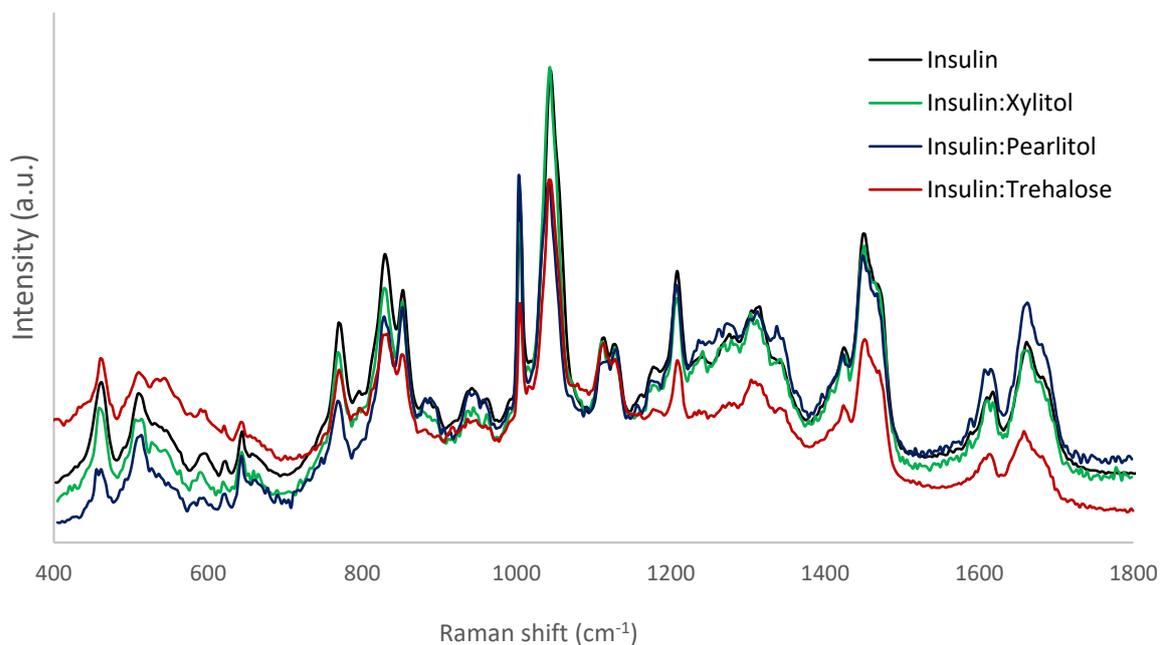

Fig.4: Raman spectra from 400 to 1800 cm-1 of pure insulin and insulin-sugars

Penetration of MN in porcine skin

The polymeric arrays featuring different MN shapes along with the metallic ones were inserted in porcine skin samples using a texture analyser. All MN designs successfully pierced the skin and no MN failure was reported. Force against displacement data were continuously recorded throughout the penetration and the data are shown in Fig. 5.
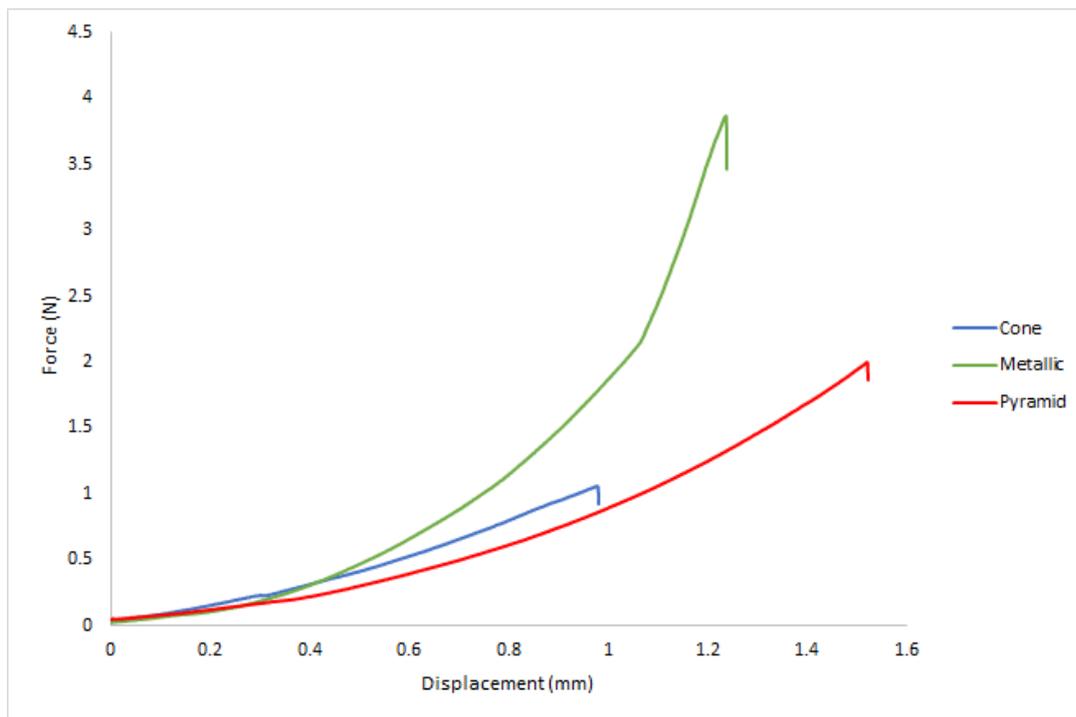
Fig. 5: Force vs displacement curves for MN penetration in porcine skin

The sharp drop of the load corresponds to the insertion of the MN into the skin (Davis et al., 2004). Prior to that event, all curves present an initial linear portion (displacement < 0.3 mm); the slope then changes constantly as the MN continues to penetrate the skin revealing a non-linear connection between the developed forces and the penetration depth.
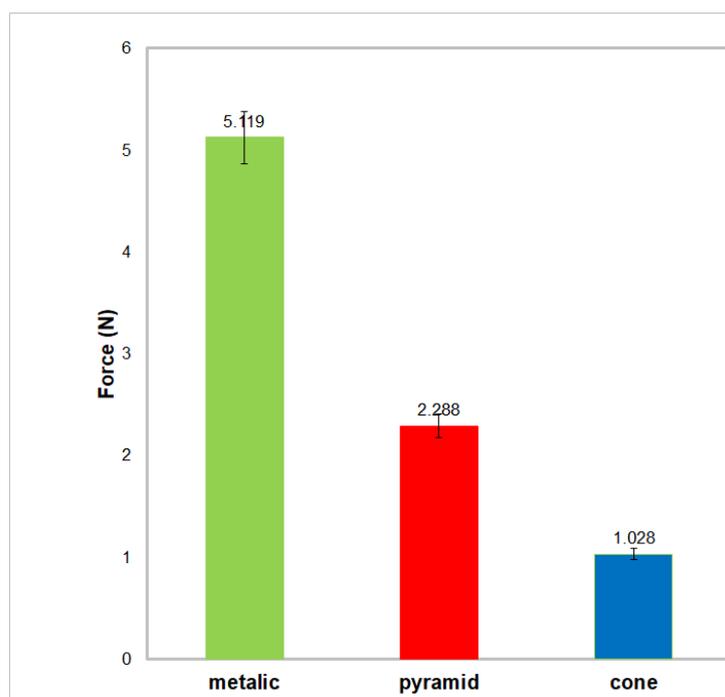

Fig. 6: Maximum forces for MN penetration in porcine skin

This behaviour could be attributed to the viscoelastic nature of the skin tissue, however indentation studies by Pailler-Mattei et al. (Pailler-Mattei et al., 2008) proposed the neglecting of the viscous part and the consideration of the skin as an elastic material in the load range of 0-20 N. Considering that all the measurements are well below the 20 N margin, a linear connection between force and displacement throughout the test should be expected. The divergence from linearity shows that the needle penetration of the skin starts earlier than the sharp drop of load. The load increases as the needle goes deeper through the skin until a threshold force is reached and insertion becomes abrupt. These findings are in accordance with the work from Gittard et al. (Gittard et al., 2013) that concluded that MN penetration should be viewed as a series of sequential penetrations until a maximum force is applied, rather than a single event. The threshold load indicates that the MN insertion is successful, and the respective values are depicted in Fig. 6.

Regarding the different designs and apart from the metallic MN that require the maximum threshold force for penetration, the cone design requires the least force to penetrate the porcine skin. Since both designs are dimensionally similar, the variation of the maximum load required for penetration can be attributed to the difference of the MN-to-skin contact area between the two designs. Indeed, Equation (1) yields a total contact surface for the cone design, of 1.76 mm^2 per needle. On the other hand, the lateral surface for pyramid is found to be 2.24 mm^2 per needle, from Equation (2).

$$S_{cone} = \pi r \sqrt{h^2 + r^2} \qquad\qquad Eq.\ (1)$$

where: r, the base radius
h, the height of the MN

$$S_{pyramid} = l\sqrt{\frac{w^2}{2} + h^2} + w\sqrt{\frac{l^2}{2} + h^2} \qquad\qquad Eq.\ (2)$$

where: l, the length of the base
w, the width of the base
h, the height of the MN

The 21% difference in area between the two designs indicates that the frictional forces after initial penetration until the threshold force in reached, are greater for the pyramid needles. As a result, greater loads are required to achieve further penetration through the skin.

Insulin release studies

In vitro insulin release studies were conducted using dermatomed porcine skin through Franz diffusion cells. The alcohol sugars (mannitol, xylitol) and the disaccharide sugar (trehalose) provided excellent coatings on the MN surface and due to their hydrophilic nature were expected to provide rapid release rates. Indeed, as shown in Fig 7a,b the observed insulin release rates in the first 2 min varied from 63 – 69% and 57 – 64% for the pyramid and cone – shaped 3D microneedles. After 20min more than 80% of insulin was detected in the receptor's compartment and 90 – 95% in 30 min. Furthermore, the release profiles were almost identical for all carries and no statistical difference was observed for each MN design (two-tail p = 0.0026). The rapid insulin profiles were attributed to the extremely high hydration rates of the

alcohol sugars and the disaccharide respectively in the porcine skin micro-cavities crated upon the MN piercing.
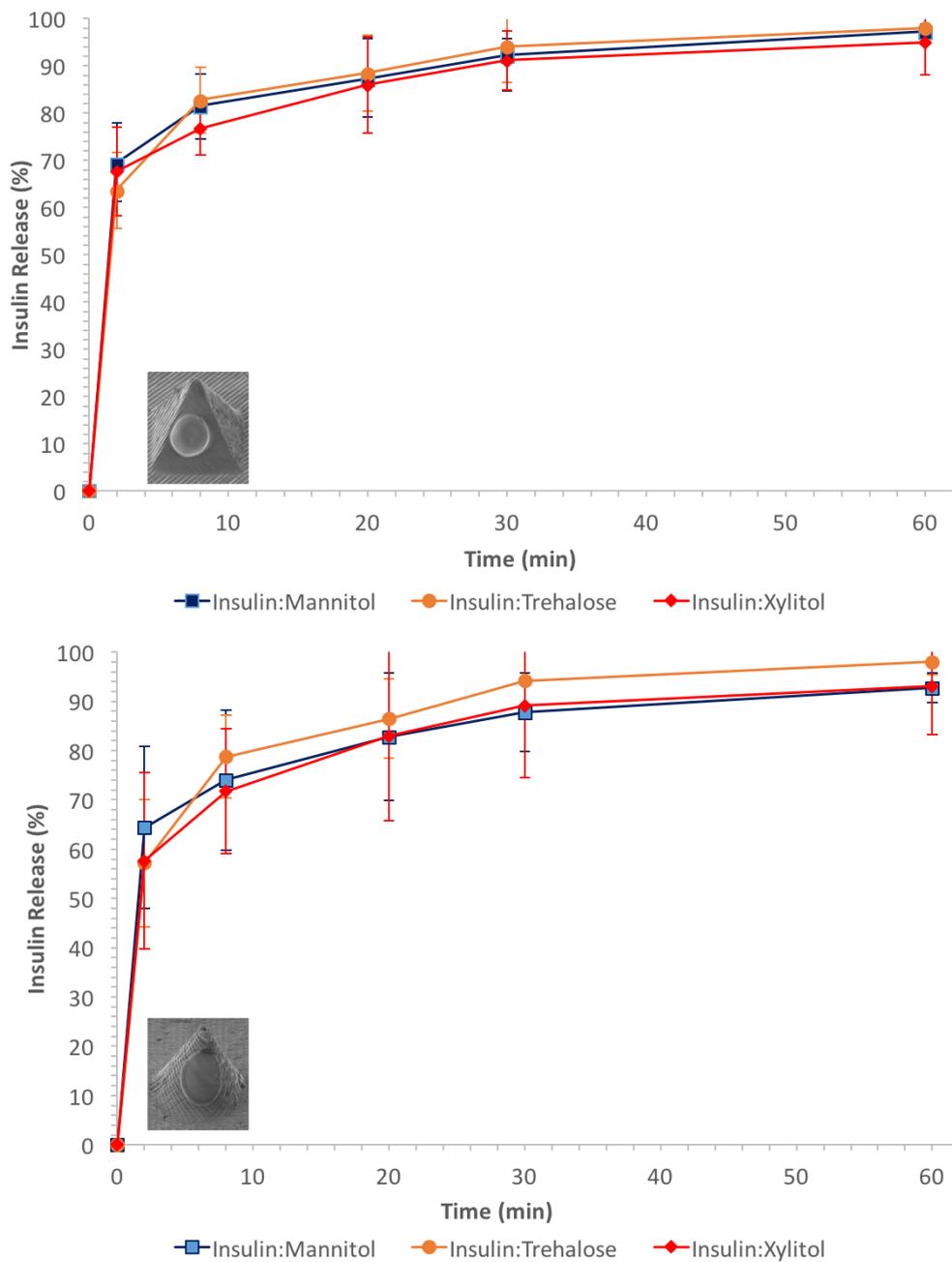

Fig. 7: Dissolution profiles of insulin 3D printed cone and pyramid – shaped microneedles

4. Conclusions

A 3D printing stereolithographic technique was introduced for the fabrication of microneedle designs for insulin delivery. SLA facilitated the printing of high quality MNs with various designs. Insulin formulations with mannitol, trehalose and xylitol were coated on the MN surface using inkjet printing to provide accurate and reproducible active coating layers. All carriers were found to preserve insulin integrity namely the α –helix and β-Sheet with

xylitol presenting the foremost performance. Franz cell diffusion studies revealed rapid insulin release rates within 30min. In conclusion, we demonstrated that 3D printing can be efficiently used for microneedle fabrication.

Acknowledgments

5. References

Alkilani AZ, McCrudden MTC, Donnelly RF (2015). Transdermal drug delivery: Innovative pharmaceutical developments based on disruption of the barrier properties of the stratum corneum. Pharmaceutics 7:438–470.

Andrade F, Fonte P, Oliva M, Videira M, Ferreira D, Sarmento B (2015). Solid state formulations composed by amphiphilic polymers for delivery of proteins: Characterization and stability. Int. J. Pharm. 486:195–206.

Carpenter JF, Crowe JH (1989). An infrared spectroscopic study of the interactions of carbohydrates with dried proteins. Biochem. 28(9):3916-22.

Chen W, Li H, Shi D, Liu Z and Yuan W (2016). Microneedles As a Delivery System for Gene Therapy. Front. Pharmacol. 7:137.

Davis SP, Landis BJ, Adams ZH, Allen MG, Prausnitz MR (2004). Insertion of microneedles into skin: Measurement and prediction of insertion force and needle fracture force. J. Biomech. 37:1155–1163.

Dillon C, Hughes H, O'Reilly NJ, McLoughlin P (2017). Formulation and characterisation of dissolving microneedles for the transdermal delivery of therapeutic peptides. Int. J. Pharm. 526:125–136.

Ettinger MJ, Timasheff SN (1971). Optical Activity of Insulin. II. Effect of Nonaqueous Solvents. Biochemistry 10(5): 831–40.

Gittard SD, Chen B, Xu H, Ovsianikov A, Chichkov BN, Monteiro-Riviere NA, Narayan RJ. 2013. The effects of geometry on skin penetration and failure of polymer microneedles. J. Adhes. Sci. Technol. 27:227–243.

Gittard SD, Miller PR, Jin C, Martin TN, Boehm RD, Chisholm BJ, Stafslien SJ, Daniels JW, Cilz N, Monteiro-Riviere NA, Nasir A, Narayan RJ (2011). Deposition of antimicrobial coatings on microstereolithography-fabricated microneedles. Jom 63:59–68.

Guo X, Wang W (2017). Challenges and recent advances in the subcutaneous delivery of insulin. Expert Opin Drug Deliv. 2017 Jun;14(6):727-734.

Hull CW (1984). Apparatus for production of three-dimensional objects by stereolithography. US 4575330 A.

Ita K (2015). Transdermal delivery of drugs with microneedles-Potential and challenges. Pharmaceutics 7:90–105.

Kaushik S, Hord AH, Denson DD, McAllister DV, Smitra S, Allen MG, Prausnitz MR (2001). Lack of pain associated with microfabricated microneedles. Anesth. Analg. 92:502–504.

Kim YH, Sioutas C, Shing KS (2009). Influence of stabilizers on the physicochemical characteristics of inhaled insulin powders produced by supercritical antisolvent process. Pharmaceutical Research 26(1):61–71.

Kodama H. A scheme for three-dimensional display by automatic fabrication of three-dimensional model. IEICE Trans. Electron. J64 (1981), 237.

Lu Y, Mantha SN, Crowder DC, Chinchilla S, Shah KN, Yun YH, Wicker RB, Choi J-W (2015). Microstereolithography and characterization of poly(propylene fumarate)-based drug-loaded microneedle arrays. Biofabrication 7(4), 045001.

McCrudden MTC, Alkilani AZ, Courtenay AJ, McCrudden CM, McCloskey B, Walker C, Alshraiedeh N, Lutton REM, Gilmore BF, Woolfson AD, Donelly RF (2015). Considerations in the sterile manufacture of polymeric microneedle arrays. Drug Deliv. Transl. Res. 5:3–14.

Melberg, Steen G., and W. Curtis Johnson (1990). "Changes in Secondary Structure Follow the Dissociation of Human Insulin Hexamers: A Circular Dichroism Study." Proteins: Structure, Function, and Bioinformatics 8(3): 280–86.

Moreno E, Schwartz J, Calvo A, Blanco L, Larrea E, Irache JM, Sanmartín C, Coulman SA, Soto M, Birchall JC, Espuelas S (2017). Skin vaccination using microneedles coated with a plasmid DNA cocktail encoding nucleosomal histones of Leishmania spp. Int. J. Pharm. 533:236–244.

Narayan RJ (2014). Transdermal delivery of insulin via microneedles. J Biomed Nanotechnol. 10(9):2244-60.

Pailler-Mattei C, Bec S, Zahouani H. 2008. In vivo measurements of the elastic mechanical properties of human skin by indentation tests. Med. Eng. Phys. 30:599–606.

Pedde RD, Mirani B, Navaei A, Styan T, Wong S, Mehrali M, Thakur A, Mohtaram NK, Bayati A, Dolatshahi-Pirouz A, Nikkhah M, Willerth SM, Akbari M (2017). Emerging Biofabrication Strategies for Engineering Complex Tissue Constructs. Adv. Mater. 29:1–27.

Pocker, Y., and Subhasis B. Biswas. 1980. Conformational Dynamics of Insulin in Solution. Circular Dichroic Studies. Biochemistry 19(22): 5043–49.

Ross S, Scoutaris N, Lamprou D, Mallinson D, Douroumis D (2015). Inkjet printing of insulin microneedles for transdermal delivery. Drug Deliv. Transl. Res. 5:451–461.

Sanjay ST, Zhou W, Dou M, Tavakoli H, Ma L, Xu F, Li XJ (2017). Recent advances of controlled drug delivery using microfluidic platforms. Adv. Drug Deliv. Rev., *In press*.

Sarmento BD, Ferreira C, Jorgensen L, van de Weert M (2007). Probing Insulin's Secondary Structure after Entrapment into Alginate/chitosan Nanoparticles. Eur. J. Pharm. Biopharm. 65(1): 10–17.

Schiffter H, Condliffe J, Vonhoff S (2010). Spray-freeze-drying of nanosuspensions: the manufacture of insulin particles for needle-free ballistic powder delivery. J. R. Soc. Interface 7:483–500

Sreerama, N. and Woody, R.W. (2000), Analytical Biochemistry, 287, 252–260.

Souillac PO, Middaugh CR, Rytting JH (2002). Investigation of Protein/carbohydrate Interactions in the Dried State. 2. Diffuse Reflectance FTIR Studies. International Journal of Pharmaceutics 235(1–2): 207–18.

Timasheff SN (1993). The control of protein stability and association by weak interactions with water: how do solvents affect these processes? Annu Rev Biophys Biomol Struct. 22:67-97.

Uddin MJ, Scoutaris N, Klepetsanis P, Chowdhry B, Prausnitz MR, Douroumis D (2015). Inkjet printing of transdermal microneedles for the delivery of anticancer agents. Int. J. Pharm. 494:593–602.

Wermeling DP, Banks SL, Hudson DA, Gill HS, Gupta J, Prausnitz MR, Stinchcomb AL (2008). Microneedles permit transdermal delivery of a skin-impermeant medication to humans. Proc. Natl. Acad. Sci. U. S. A. 105:2058–63.

Yao G, Quan G, Lin S, Peng T, Wang Q, Ran H, Chen H, Zhang Q, Wang L, Pan X, Wu C (2017). Novel dissolving microneedles for enhanced transdermal delivery of levonorgestrel: In vitro and in vivo characterization. Int. J. Pharm. 534:378–386.

Yong Z, Yingjie D, Xueli W, Jinghua X, Zhengqiang L (2009). Conformational and bioactivity analysis of insulin: Freeze-drying TBA/water co-solvent system in the presence of surfactant and sugar. Int. J. Pharm. 371:71–81

Yu NT, Liu SC, O'Shea DC (1972). Laser Raman Spectroscopy and the Conformation and Proinsulin of Insulin. J. Mol. Biol. 70(1): 117–32.

Yu W, Jiang G, Liu D, Li L, Chen H, Liu Y, Huang Q, Tong Z, Yao J, Kong X (2017). Fabrication of biodegradable composite microneedles based on calcium sulfate and gelatin for transdermal delivery of insulin. Mater. Sci. Eng. C 71:725–734.

Yu W, Jiang G, Zhang Y, Liu D, Xu B, Zhou J (2017). Polymer microneedles fabricated from alginate and hyaluronate for transdermal delivery of insulin. Mater. Sci. Eng. C 80:187–196.

Yu NT, Liu SC, O'Shea DC (1972). Laser Raman Spectroscopy and the Conformation and Proinsulin of Insulin. J. Mol. Biol. 70(1): 117–32.